PNAS
www.pnas.org

Supplementary Information for

Solidification and superlubricity with molecular alkane films

Alexander M. Smith, James E. Hallett and Susan Perkin

Susan Perkin.
E-mail: susan.perkin@chem.ox.ac.uk

This PDF file includes:

Supplementary text
Figs. S1 to S3
References for SI reference citations

Supporting Information Text

Oscillatory Forces. In this section we discuss in further detail the oscillatory structural forces as reported in Fig.1 of the main text. In agreement with previous SFA literature, the measured repulsive force maxima of the innermost oscillations were found to vary depending on the approach rate of the surfaces, with faster approaches resulting in higher measured forces. This is due to elastic deformation of the glue behind the mica pieces before drainage of the confined liquid occurs. As a result of this small flattening of the curved surfaces, values of F_N/R are overestimated for values > 2 mN m^{-1} which for dodecane is typically when D < 2 nm. The adhesive minima are unaffected by this, and hence used to obtain the decay length of the oscillatory envelope. The attractive van der Waals force is negligible compared to the structural forces, hence we fit the force profiles with a simple damped cosine wave:

$$F_N/R = Ae^{-D/\lambda_o}cos(\omega D + \phi) \quad [1]$$

with $\lambda_o = 0.51$ nm and $2\pi/\omega = 0.49$ nm. Normal forces between macroscopic particles or surfaces across simple molecular liquids are expected to follow an exponentially decaying oscillatory function with parameters λ_o and $2\pi/\omega$ determined solely by the radial distribution function in the bulk fluid (1). Indeed, we find that these parameters are insensitive to the relative orientation of the mica sheets, or even the confining material itself provided it is sufficiently smooth. Figure S1 shows the measured minima of the oscillatory forces for aligned and misaligned mica surfaces, and also compares to experiments where the mica surfaces were coated with molecularly smooth amorphous OTE (octadecyltriethoxysilane) monolayers. It is clear from Figure S1 that the magnitude and location of the adhesive minima are similar, within the scatter of the experiment, in each case. We note that an earlier careful study of the adhesion between mica surfaces as a function of their twist angle was performed by McGuiggan and Israelachvili(2), and there it was found that a striking increase of adhesion was found at angles very close to $\theta = 0^\circ$ in water and electrolytes. However in air there was no such affect. Those authors did not study hydrocarbon films, and it appears that the enhancement of adhesion at commensurate orientation in their experiments may be particular to aqueous systems.

Friction across dodecane confined between OTE monolayers. In the main text we provide evidence for a strong effect of the twist angle between the two confining mica sheets on the friction measured across the confined dodecane film. This led to the hypothesis (also supported by various simulation studies in the literature, as referred to in the main text) that the solidified dodecane film lies in commensurate orientation with one mica surface (if the mica crystals are out of registry) or both mica surfaces (if the two mica surfaces are aligned). This explains the high friction coefficient, and solidification at larger film thicknesses, when the two mica sheets are in crystallographic alignment; and ultra-low friction when the two mica sheets are misaligned. In order to test this hypothesis we carried out friction experiments with the mica surfaces coated in an atomically-smooth amorphous OTE monolayer; see Figure S2.

In contrast to experiments with bare crystalline mica surfaces, we found no effect of twist angle on friction forces measured between the smooth OTE monolayers across the dodecane film confined to a single molecular layer. Figure S2 shows a representative example of the transition from viscous (liquid-like) to elastic (solid-like) shear response upon confining the dodecane film from two to one molecular layer. Both the friction coefficient and magnitude of friction forces are extremely similar irrespective of the twist angle of the underlying mica substrates. As noted above, the oscillatory structural forces are identical within our resolution with and without OTE layers; thus direct comparison of mica and OTE-coated-mica on the friction can be attributed to their surface structure rather than an indirect effect on the layering. The test experiment with OTE-coated mica – where crystalline structure is not present on the surfaces – supports the hypothesis that laterally-ordered domains in the dodecane can align with the crystalline structure on one or both mica surfaces, depending on their relative orientation, and this determines the resulting friction.

We also note that, due to the hydrophobic nature of the OTE monolayers the friction forces were largely unaffected by ambient lab humidity, and were reproducible between different experiments. As we show in the main text, this is not the case for mica surfaces, which show a dramatic effect of adsorbed water at the surfaces. Although P_2O_5 is frequently used in the measurement chamber, it only prevents the liquid from getting wetter and unlikely to dry it. In particular, once water is adsorbed at the hydrophilic surfaces before immersion in the alkane it is very unlikely to then go into the bulk liquid. Crucially, the result of this is that the presence of small amounts of water adsorbed from ambient lab air can cause enormous increases in friction even when using liquids which are themselves as dry as possible. The origin of this high friction in the presence of adsorbed water is not clear but may be related to the formation of nm-sized crystallites of K_2CO_3 or $KHCO_3$ through reaction of mica surface K^+ ions with dissolved carbonaceous gases catalysed by water(3).

Notes on method of mica surface preparation. Importantly, the ultra-low friction behaviour reported here for misaligned surfaces can be achieved using mica cleaved and cut with Pt wire using standard procedures with careful consideration of laminar flow(4), and without the need for prior re-cleaving of the mica surfaces. However a low humidity in the lab is required (in our experiments RH <20%) for the duration of surface preparation, which must be kept as short as possible before mounting lenses in the dry measurement chamber. Without such precautions or prior re-cleaving, friction coefficients for dodecane confined between mica surfaces are typically in the range $0.1 < \mu < 2$.

Notes on method of determining the film thickness, D, in cases of an asymmetric 3-layer interferometer. In many of the present experiments the mica sheets were re-cleaved with tape using the method of Frantz and Salmeron(5). In this case the thickness of the two mica sheets can be unequal. The optical cavity for FECO measurement of D is then asymmetric. However, for the

present experiments where the range of D of interest is $0 < D < 10$ nm and the refractive index of the fluid (dodecane) and mica are similar, the error in calculating D using the analytic equation for a *symmetric* interferometer(6) is negligible and this is what we have done in the present experiments. Here, we explain this further and justify our method by presenting a full multilayer matrix method fit using an asymmetric mica(T_1)-liquid-mica(T_2) stack, and find that in the range of separations relevant to this study (< 100 nm), there is little difference between the symmetrical analytical equation and asymmetrical multilayer matrix method, most particlarly for the degree of asymmetry and gap refractive index studied here.

Extent of asymmetry. We begin by note that the asymmetry in experiments performed in this way is mild. When re-cleaving the mica surface using Kapton tape, the exfoliated mica surface remains attached to the tape and its approximate thickness can be inferred from its colour. We typically find that the exfoliated mica layers from both lenses are of similar colour, indicating that the remaining mica pieces on both lenses are of comparable thickness.

Previous work informing our methodology. While the work of Israelachvili(6) (and later further described by Tadmor, Chen and Israelachvili(7)) established the widely-used analytical method to determine liquid layer thickness in a symmetrical three layer interferometer (s3LI), there has been a considerable effort to both improve the accuracy of the analytical method, and to also determine gap separations for other optical stacks beyond the s3LI.

The multilayer matrix method, outlined with reference to surface force measurements by Clarkson(8) can be used to determine the transmitted spectrum of an arbitrary optical stack. Each individual layer has a corresponding optical matrix that depends on the layer thickness, complex refractive index, wavelength, incident angle (for the crossed cylinder geometry of the SFB, this is taken as 0°), dielectric permittivity and magnetic permeability. The total transmission spectrum can then be determined from the matrix product of all the layers in the stack. Further details are given by Balabajew(9). Recent work has utilised the multi matrix method to perform contact-free calibration, for systems where an air-contact calibration could result in irreversible substrate damage(9), and to determine separation in an asymmetric "three mirror" interferometer(10). However, rather than an analytical relationship between fringe position and gap thickness, the MMM requires a brute force process of generating many transmission spectra to best match the experimental data, which had previously limited its use as a direct fitting method.

Horn and Smith(11) derived equations for asymmetric interferometers where the substrates are of different thickness, with different refractive index, or both. In order to determine the gap thickness, the estimated thickness asymmetry is estimated and then refined via an iterative process. They found that this process yields excellent agreement with numerical solutions found via the multilayer matrix method.

It was noted by Israelachvili that the thickness obtained via contact calibration of a three layer interferometer does not yield the true mica thickness but rather an effective "optical" thickness, due to phase change at the mica-silver interface, and a correction factor was introduced to accommodate this. Farrell, Bailey and Chapman(12) extended this work, and explicitly calculated the different gap thicknesses if phase changes were included or neglected.

Direct comparison of MMM to symmetric analytic method. We now proceed to explore the suitability of using the analytical relationship for a symmetrical interferometer to study a potentially asymmetric system. Figure S3a shows the contact calibration for a dataset used in this study. We assign the left hand fringe to be the p-fringe and note it is of odd order due to its shape. The transmission spectrum was recorded at several distances and the separation was determined using both the analytical relationship and using the MMM (figure S3b) as follows: Optical properties of silver(13) and mica(14) are obtained from the literature. The contact calibration thickness T is used to constrain the thickness of the two mica layers, such that $T = T_1 + T_2$. Using the separations obtained from the analytical symmetrical relationship as a first estimate, we refine both the gap separation and asymmetry$r = (T_1/(T_1 + T_2))$ for the away-from-contact data by comparison to MMM-generated spectra and minimisation of their sum-squared residuals. Clarkson(8) noted an oscillatory movement of fringe position with asymmetry for a fixed separation, such that a given p and $p - 1$ fringe position can correspond to multiple asymmetries and separations. We also note this when fitting experimental spectra, and show that multiple asymmetries yield near-equally good fits to the data, but crucially also result in the same fitted separation. Nevertheless a global fit of multiple separations reveals that r =0.5865 yields the best overall fit, so we take this value throughout. Despite this fitted asymmetry, there is good agreement between the separations determined by fitting the whole spectrum with an asymmetric stack, and those determined analytically from the p-fringe position, assuming a symmetric stack. Indeed, the agreement is excellent and differs by no more than a few Angstroms even at separations in excess of 70 nm (figure S3e, solid points).

While this agreement is gratifying, one might naively find it surprising. We therefore also make some general observations about the applicability of the symmetrical analytical expression for asymmetric systems. Figure S3d shows the transmission peak positions for different separations for a symmetric and asymmetric three layer interferometer of the same thickness and optical properties as the one used in the example above. We note that, for the same fringe order, the behaviour of the symmetric (pink) and asymmetric (blue) fringes are notably different. Why should this then yield the same fitted separation? Clarkson(8) notes "the curve for the odd fringe... has opposite curvature to the curve for the odd fringe for the symmetrical case, and similarly for the even fringes". Similarly Horn and Smith also note(11) that the curvature of even and odd fringes can change in asymmetric systems. Indeed, as shown in figure S3e, fitting the MMM symmetric interferometer (pink dots) with the analytical method requires the p-fringe to be even, but using the analytical method to fit the MMM asymmetric interfometer (blue dots) for an even p-fringe results in poor agreement between the MMM thickness and the fitted thickness. On the other hand, by assuming the p-fringe to be odd (figure S3e, blue line, as implied from figure S3a.), we find excellent agreement between the two fits, confirming the applicability of the symmetric analytical form for asymmetric systems. In the limiting case of complete asymmetry, i.e. a two layer interferometer, all fringes regardless of order are "even" in that separation always depends on the refractive index of the medium, so it is necessary to use a different analytical expression. However, for the case of small

asymmetry (aided by the relatively small refractive index mismatch between mica and dodecane as opposed to, say, mica and water or mica and air) as shown here, using the relationship for the symmetric interferometer remains appropriate.

Note on the observed 'quantized friction'. Our measurements of friction as a function of load suggest that the friction across dodecane is load dependent but also quantized with respect to the number of confined molecular layers: see examples in Fig.2 (d),(i) in the main text. Such *quantized friction* has been demonstrated in the past for non-polar liquid(15) and for ionic liquid(16). We note that the change in contact area with applied normal load in the present experiments is weak and is not sufficient to account for the increase in friction with load, i.e., the shear stress also increases with load. The friction coefficients measured here appear to be approximately constant within each experiment, i.e. not varying with the number of confined layers, and only the *adhesion contribution* to the friction force varies with film thickness. This latter aspect is expected from the oscillatory nature of the force profiles: the adhesive contribution to friction increasing with decreasing film thickness, in discrete steps as each layer of liquid is squeezed from the film, resulting in step-changes in friction.

Requests for data and further details. Raw data and further details of protocols are available upon reasonable request to the authors.

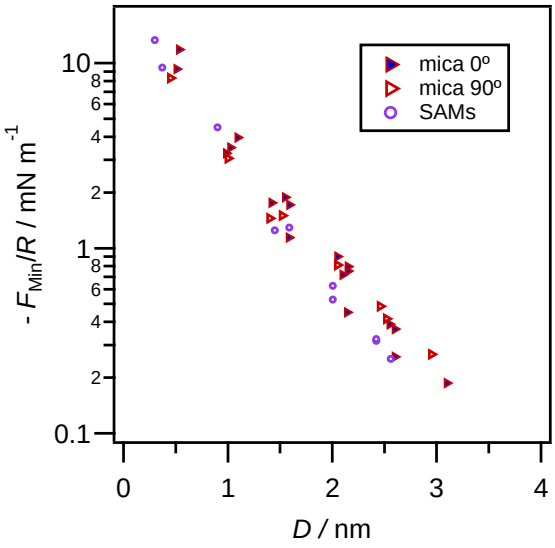

Fig. S1. Adhesive minima measured on retraction of aligned mica surfaces ($\theta = 0\,\mathrm{deg}$), misaligned mica surfaces ($\theta = 90\,\mathrm{deg}$) and smooth Self-Assembled Monolayers (SAMs) of OTE across molecularly confined dodecane films.

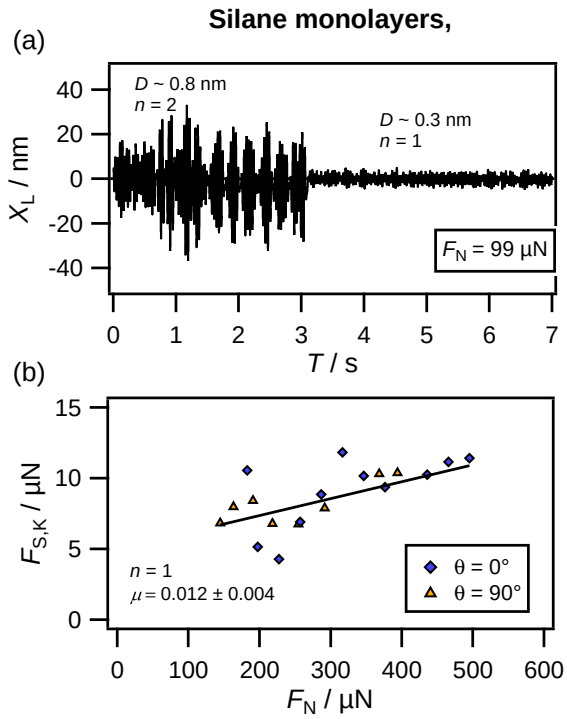

Fig. S2. (a) Variation of the lateral force, FL, transmitted between OTE monolayers across dodecane films of thickness n molecular layers due to ambient vibrations as a function of time, during the transition from n = 2 to n = 1. (b) Variation of kinetic shear force, $F_{S,K}$, with normal force, F_N, for different mica alignments.

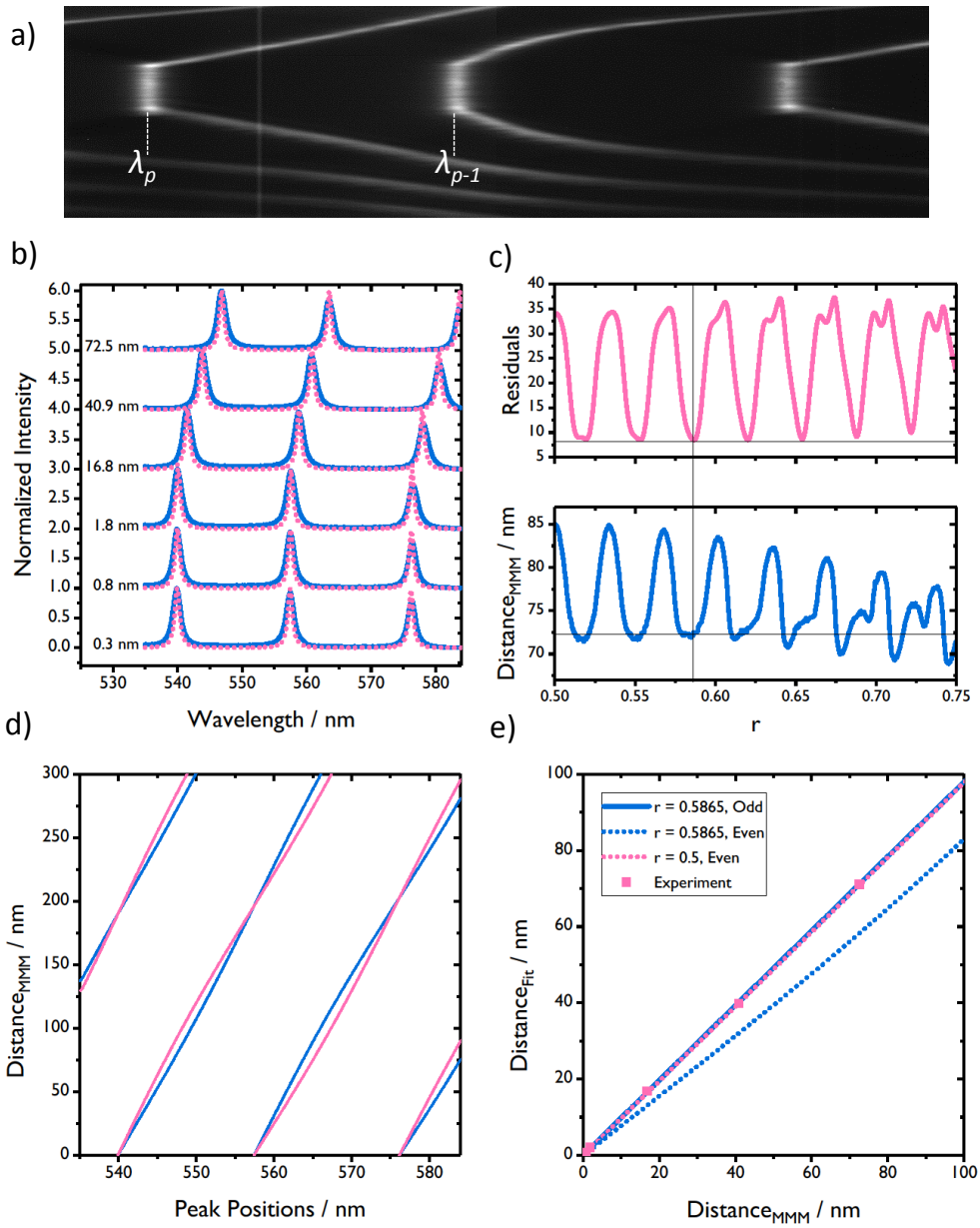

Fig. S3. a) Transmission spectrum for crystallographically mis-aligned mica at contact. p and p-1 fringes are indicated, of apparent odd and even order respectively. b) Transmission spectra traces at various surface separations (blue solid) and corresponding MMM fits for an asymmetry of 0.5865 (pink dotted) with gap separation of fit also shown. c) Example fitting residuals and corresponding gap separation for most distant trace from b). Solid line indicates global residual minimum and corresponding distance. Note that other values of r produce similarly good fits, but result in essentially the same gap separation. d) Numerically modelled transmission spectrum peak positions for different separations, for the same T as a), but for symmetric mica layers (pink) and asymmetric (r=0.5865, blue). e) Distances obtained from analytical fit of d), as function of MMM distance. Pink dotted line corresponds to the symmetric mica case, which is of even fringe order. Blue dotted line is for asymmetric mica case, assuming even fringe order. Blue solid line is for asymmetric mica, assuming odd fringe order (as implied by a)). Pink squares correspond to distances obtained using analytical fit and MMM shown in b), demonstrating excellent agreement between the two methods.

References

1. R Evans, J Henderson, D Hoyle, A Parry, Z Sabeur, Asymptotic decay of liquid structure: oscillatory liquid-vapour density profiles and the fisher-widom line. *Mol. Phys.* **80**, 755–775 (1993).
2. PM McGuiggan, JN Israelachvili, Adhesion and short-range forces between surfaces. part ii: Effects of surface lattice mismatch. *J. Mater. Res.* **5**, 2232–2243 (1990).
3. HK Christenson, NH Thomson, The nature of the air-cleaved mica surface. *Surf. Sci. Reports* **71**, 367 – 390 (2016).
4. S Perkin, et al., Forces between mica surfaces, prepared in different ways, across aqueous and nonaqueous liquids confined to molecularly thin films. *Langmuir* **22**, 6142–6152 (2006).
5. P Frantz, M Salmeron, Preparation of mica surfaces for enhanced resolution and cleanliness in the surface forces apparatus. *Tribol. Lett.* **5**, 151–153 (1998).
6. J Israelachvili, Thin-film studies using multiple-beam interferometry. *J. Colloid Interface Sci.* **44**, 259–272 (1973).
7. R Tadmor, N Chen, JN Israelachvili, Thickness and refractive index measurements using multiple beam interference fringes (feco). *J. Colloid Interface Sci.* **264**, 548 – 553 (2003).
8. MT Clarkson, Multiple-beam interferometry with thin metal films and unsymmetrical systems. *J. Phys. D: Appl. Phys.* **22**, 475–482 (1989).
9. M Balabajew, CD van Engers, S Perkin, Contact-free calibration of an asymmetric multi-layer interferometer for the surface force balance. *Rev. Sci. Instruments* **88**, 123903 (2017).
10. CD van Engers, M Balabajew, A Southam, S Perkin, A 3-mirror surface force balance for the investigation of fluids confined to nanoscale films between two ultra-smooth polarizable electrodes. *Rev. Sci. Instruments* **89**, 123901 (2018).
11. RG Horn, DT Smith, Analytic solution for the three-layer multiple beam interferometer. *Appl. Opt.* **30**, 59–65 (1991).
12. B Farrell, AI Bailey, D Chapman, Experimental phase changes at the mica–silver interface illustrate the experimental accuracy of the central film thickness in a symmetrical three-layer interferometer. *Appl. Opt.* **34**, 2914–2920 (1995).
13. KM McPeak, et al., Plasmonic films can easily be better: Rules and recipes. *ACS Photonics* **2**, 326–333 (2015).
14. DF Kienle, JV de Souza, EB Watkins, TL Kuhl, Thickness and refractive index of dppc and dppe monolayers by multiple-beam interferometry. *Anal. Bioanal. Chem.* **406**, 4725–4733 (2014).
15. E Kumacheva, J Klein, Simple liquids confined to molecularly thin layers. ii. shear and frictional behavior of solidified films. *J. Chem. Phys.* **108**, 7010–7022 (1998).
16. AM Smith, KRJ Lovelock, NN Gosvami, T Welton, S Perkin, Quantized friction across ionic liquid thin films. *Phys. Chem. Chem. Phys.* **15**, 15317–15320 (2013).